Metallization of solid molecular hydrogen in two dimensions: Mott-Hubbard-type transition

Andrzej Biborski,[1,*] Andrzej P. Kądzielawa,[2,†] and Józef Spałek[2,‡]

[1]*Academic Centre for Materials and Nanotechnology, AGH University of Science and Technology, al. Mickiewicza 30, PL-30-059 Kraków, Poland*

[2]*Marian Smoluchowski Institute of Physics, Jagiellonian University, ulica Łojasiewicza 11, PL-30-348 Kraków, Poland*

(Received 22 February 2017; published 1 August 2017)

We analyze the pressure-induced metal-insulator transition in a two-dimensional vertical stack of H_2 molecules in (x-y) plane, and show that it represents a striking example of the Mott-Hubbard-type transition. Our combined exact diagonalization approach, formulated and solved in the second quantization formalism, includes also simultaneous *ab initio* readjustment of the single-particle wave functions, contained in the model microscopic parameters. The system is studied as a function of applied side force (generalized pressure), both in the H_2-molecular and H-quasiatomic states. Extended Hubbard model is taken at the start, together with longer-range electron-electron interactions incorporated into the scheme. The stacked molecular plane transforms discontinuously into a (quasi)atomic state under the applied force via a two-step transition: the first between molecular insulating phases and the second from the molecular to the quasiatomic metallic phase. No quasiatomic insulating phase occurs. All the transitions are accompanied by abrupt changes of the bond length and the intermolecular distance (lattice parameter), as well as by discontinuous changes of the principal electronic properties, which are characteristic of the Mott-Hubbard transition here associated with the jumps of the predetermined equilibrium lattice parameter and the effective bond length. The phase transition can be interpreted in terms of the solid hydrogen metallization under pressure exerted by, e.g., the substrate covered with a monomolecular H_2 film of the vertically stacked molecules. Both the Mott and Hubbard criteria at the insulator to metal transition are discussed.

DOI: 10.1103/PhysRevB.96.085101

I. MOTIVATION

Hydrogen is the first and the simplest of elements in the Periodic Table, with an elementary structure of the energy levels. Also, the H_2 molecule represents the testing ground of quantum-mechanical methods [1,2]. This elementary nature of the atomic or molecular energy levels transforms into an involved manifold of states and available energies as exemplified by the abundance of their condensed liquid and solid phases [3,4]. The resultant phase diagram is complex, and the catalog of observed phases—especially of the solid ones—steadily increases [3,5]. The lack of clarity concerning their crystal structure in many cases is intimately connected with an incomplete insight into their electronic properties. However, it has been unclear until very recently [6] whether the solid-hydrogen atomic and metallic phase may indeed exist. Nonetheless, the detailed nature of this transition from an insulating molecular phase to the (quasi-)metallic atomic state, is still under debate [7,8], starting from the historic paper by Wigner and Huntington [9]. Once confirmed [10], the recent work [6] would represent a decisive step in achieving our understanding of the metallization of molecular hydrogen both experimentally and theoretically. However, the claim [6] must first be supported by refutation of the objections [10,11]. The fundamental question is whether this transition is of the Mott-Hubbard type, i.e., driven principally by the interelectronic correlations [12,13] or is it in class of general dielectric–metal transition driven simply by the formation of overlapping bands under strong pressure [14,15]. The principal purpose of the present paper is to provide an affirmative answer to the former possibility, albeit limited to a two-dimensional situation.

Our discussion of the problem is based on an original method of approach, so it is proper to sketch first the context of the current theoretical methods applied. Many, if not most of the attempts performed up to now are based on the *density functional theory* (DFT) approach. However, as it was reported by Azadi *et al.* [16], the results coming from the DFT are often ambiguous and depend strongly on a selection of the form of the *correlation-exchange* potential. Furthermore, obtaining a proper asymptotic behavior (i.e., the value of the dissociation energy) for the H_2 molecule in the large-intermolecular-separation limit is also questionable, or at least not straightforward within that approach. Whereas a proper description of the dissociation is crucial for the proper description of the metallization, as well as for the molecular crystal stabilization by taking into account the long-range London dispersion forces, a proper account of the *electron-electron* correlations is regarded by us as equally important. Also, the DFT-based methods such as LDA+U, LDA+DMFT suffer from the so-called *double-counting* problem, making their usability still somewhat limited for low-dimensional systems. In this work we apply a specific, in principle *rigorous method*, called the EDABI (Exact Diagonalization *Ab Initio* method) which allows one to surpass the last difficulty [17–20]. Most importantly, in distinction with the just mentioned methods, we calculate both single-particle wave functions (and thus the microscopic parameters of the interaction) within a single scheme, i.e., minimally go beyond the parametrized models such as Hubbard, Anderson, etc. However, the scope of this work is more general. Explicitly, we treat carefully the interelectronic interactions in the second quantization scheme

*andrzej.biborski@agh.edu.pl
†kadzielawa@th.if.uj.edu.pl
‡jozef.spalek@uj.edu.pl

 ©2017 American Physical Society

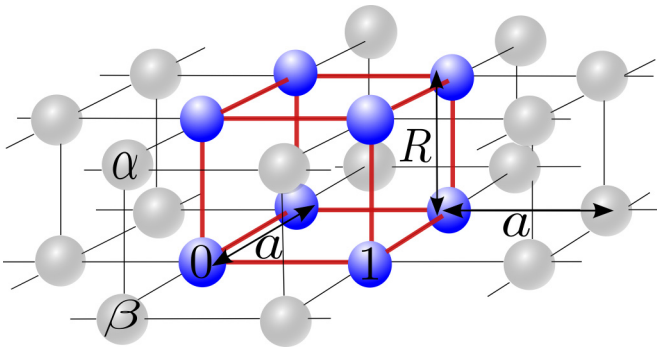

FIG. 1. Schematic representation of stacked vertically H_2 molecular 2D layer forming square lattice. The bond length and the intermolecular distance are marked by R and a, respectively. There are eight atoms in the supercell (dark blue spheres). The supercell is repeated periodically to conform periodic boundary conditions (PBC). Shaded spheres indicate atoms which are continuations resulting from the PBC implementation. The indices α, β distinguish the component atoms of each molecule.

and concurrently readjust variationally the single-particle wave functions, contained in the microscopic parameters, when constructing the resultant system correlated state. This method of approach thus inverts the order of executing the whole program of determining the electronic properties by diagonalizing the Hamiltonian including interactions in the second-quantization language and determining concomitantly the single-particle wave functions. Also, the present work is an essential extension of our recent Rapid Communication [17] on a quasi-one-dimensional hydrogen ladder to the two-dimensional (2D) situation. Namely, we provide details of both the general methodological aspects of our approach and the concrete results for the 2D stack of H_2 molecules (depicted schematically in Fig. 1). We map the whole problem onto the *extended Hubbard* model in which we additionally include the long-range (intermolecular) nature of interaction between electrons. From this point of view, we investigate the physical properties in an *exact manner* within the decomposition of the whole system into periodic units, each containing four molecules and include interatomic Coulomb interactions between the eight-atom clusters. In particular, we focus on the Mott-Hubbard physics of the system by generalizing it to the situation when an insulating and *diamagnetic* molecular 2D solid transforms into a paramagnetic atomic and metallic bilayer of H atoms.

The structure of the paper is as follows. In the following section we provide a description of the applied methodology and detail the model. Next, we discuss the phase transition induced by an external side force (effective pressure) and relate it to that of the Mott-Hubbard transition for correlated systems. Finally, we discuss a possible extension of the method to the three-dimensional (3D) systems which represent a final, not yet achieved goal within our method.

II. METHOD: EXACT DIAGONALIZATION *ab initio* APPROACH (EDABI)

Our methodology of approach is based on the variational approach which is an extension of the scheme elaborated earlier in our group exact diagonalization *ab initio* (EDABI) in the following manner [17–20]. EDABI combines both the first- and the second-quantization schemes. What is fundamentally important is that in this work we go both beyond the parametrized-model methodology [21–23] and put the emphasis first on the interelectronic correlations and simultaneously renormalize the single-particle wave functions when constructing the resultant correlated state. To achieve this goal we start with the general electronic Hamiltonian in a second-quantization form representing an interacting system of fermions [24], i.e.,

$$\hat{\mathcal{H}} = \sum_{\sigma} \int d^3r\, \hat{\Psi}^{\dagger}_{\sigma}(\mathbf{r}) \hat{\mathcal{H}}_1(\mathbf{r}) \hat{\Psi}_{\sigma}(\mathbf{r}) + \frac{1}{2} \sum_{\sigma\sigma'} \iint d^3r\, d^3r' \times \hat{\Psi}^{\dagger}_{\sigma}(\mathbf{r}) \hat{\Psi}^{\dagger}_{\sigma'}(\mathbf{r}') \hat{V}(\mathbf{r}-\mathbf{r}') \hat{\Psi}_{\sigma'}(\mathbf{r}') \hat{\Psi}_{\sigma}(\mathbf{r}). \quad (1)$$

Hamiltonians in the first (canonical) quantization are for single ($\hat{\mathcal{H}}_1$) and pair of particles [$\hat{V}(\mathbf{r}-\mathbf{r}')$], respectively. $\hat{\Psi}_{\sigma}(\mathbf{r})$ and $\hat{\Psi}^{\dagger}_{\sigma}(\mathbf{r})$ are the field operator and its adjoint, respectively. By introducing fermionic creation and anihilation operators ($\hat{c}^{\dagger}_{i\sigma}$ and $\hat{c}_{i\sigma}$), conforming the usual anticommutation relations

$$\{\hat{c}^{\dagger}_{i\sigma}, \hat{c}^{\dagger}_{j\sigma'}\} \equiv \{\hat{c}_{i\sigma}, \hat{c}_{j\sigma'}\} \equiv 0 \quad \text{and} \quad \{\hat{c}^{\dagger}_{i\sigma}, \hat{c}_{j\sigma'}\} \equiv \delta_{ij}\delta_{\sigma\sigma'}, \quad (2)$$

where σ denotes spin variable, the field operators can be represented by an expansion in the creation (annihilation) operators, weighted with the amplitudes which represent single-particle wave functions $\{w_i(\mathbf{r})\}$ forming a complete and orthogonal basis in the Hilbert space, i.e.,

$$\hat{\Psi}_{\sigma}(\mathbf{r}) = \sum_i w_i(\mathbf{r}) \hat{c}_{i\sigma}, \quad \hat{\Psi}^{\dagger}_{\sigma}(\mathbf{r}) = \sum_i w_i(\mathbf{r}) \hat{c}^{\dagger}_{i\sigma}. \quad (3)$$

Hamiltonian (1) consists of one-electron part associated with the Hamiltonian for a single particle

$$\hat{\mathcal{H}}_1(\mathbf{r}) \overset{a.u.}{=} -\nabla^2 - \sum_{i=1}^{N_S} \frac{2}{|\mathbf{R_i} - \mathbf{r}|}, \quad (4)$$

where $\mathbf{R_i}$ refers to the coordination of atomic center and N_S is the number of sites, and of the *electron-electron* interaction part

$$\hat{V}(\mathbf{r}-\mathbf{r}') \overset{a.u.}{=} \frac{2}{|\mathbf{r}-\mathbf{r}'|}. \quad (5)$$

In both equations we used atomic units (a.u). Combining Eqs. (1) and (3) leads to the Hamiltonian expressed in the language of creation and annihilation operators in the usual form

$$\hat{\mathcal{H}} = \sum_{ij} \sum_{\sigma} t_{ij} \hat{c}^{\dagger}_{i\sigma} \hat{c}_{j\sigma} + \sum_{ijkl} \sum_{\sigma,\sigma'} V_{ijkl} \hat{c}^{\dagger}_{i\sigma} \hat{c}^{\dagger}_{j\sigma'} \hat{c}_{l\sigma'} \hat{c}_{k\sigma}, \quad (6)$$

where t_{ij} and V_{ijkl} are one- and two-electron interaction parameters defined as

$$t_{ij} \equiv \langle w_i(\mathbf{r}) | \hat{\mathcal{H}}_1 | w_j(\mathbf{r}) \rangle = \int d^3r\, w^*_i(\mathbf{r}) \hat{\mathcal{H}}_1(\mathbf{r}) w_j(\mathbf{r}), \quad (7a)$$

$$V_{ijkl} \equiv \langle w_i(\mathbf{r}) w_j(\mathbf{r}') | \hat{V} | w_k(\mathbf{r}) w_l(\mathbf{r}') \rangle = \iint d^3r\, d^3r' w^*_i(\mathbf{r}) w^*_j(\mathbf{r}') \hat{V}(\mathbf{r}-\mathbf{r}') w_k(\mathbf{r}) w_l(\mathbf{r}'). \quad (7b)$$

In the computationally tractable scheme expansion (3) is truncated, i.e., the sum in (3) is assumed as *finite*. Additionally, the functions $\{w_i(\mathbf{r})\}$ in the expansion have their own, or may be supplied with, *internal* parameters $\{\lambda\}$, in addition to the quantum numbers characterized by the set $\{i\}$. These parameters might be used in the variational procedure to optimize the finite-size basis composing an approximate form of $\hat{\Psi}_\sigma$, in the correlated state, i.e.,

$$\hat{\Psi}_\sigma(\mathbf{r}) \approx \sum_i^M w_i^{(\{\lambda\})}(\mathbf{r})\hat{c}_{i\sigma}, \tag{8}$$

where M is a finite number. In that situation,the integrals defined in (7) depend also on $\{\lambda\}$ and, in effect, we obtain a *trial Hamiltonian* $\hat{\mathcal{H}}^{(\{\lambda\})}$, for which we solve the eigenequation (in our case by means of the Lanczos diagonalization method) for the many-electron problem, i.e.,

$$\hat{\mathcal{H}}^{(\{\lambda\})}\left|\Psi_T^{(\{\lambda\})}\right\rangle = E_T^{(\{\lambda\})}\left|\Psi_T^{(\{\lambda\})}\right\rangle, \tag{9}$$

where $E_T^{(\{\lambda\})}$ is a trial eigenvalue related to the $|\Psi_T^{(\{\lambda\})}\rangle$ trial many-body state. The variational procedure relies on finding the minimum of $E_T^{(\{\lambda\})}$ with respect to $\{\lambda\}$. Accordingly, the procedure is limited to relatively small systems, containing typically over a dozen electrons and corresponding single-particle states, providing an *exact* solution, at least in principle. As we have shown previously [18], the calculation of integrals (7) can be expensive in terms of the computational time. Below we provide the procedure of evaluating them. Note that the diagonal hopping element t_{ii}, i.e., the single-particle atomic energy, is also important here as we discuss the system evolution with pressure which alters also the atomic energy.

III. STARTING SYSTEM: TWO-DIMENSIONAL STACK OF H_2 MOLECULES

We consider hydrogen molecules stacked vertically on a 2D square (x-y) lattice (cf. Fig. 1). This 2D molecular crystal is parametrized by the bond length R and the intermolecular distance (lattice parameter) a. It must be stressed that even though we consider a *finite* system, we emulate the translational invariance by imposing the periodic boundary conditions (PBC). The supercell contains four H_2 molecules. Let us assign each molecule in the lattice by integers $1,2,3,\ldots i,j,k$, etc. Additionally, we introduce the indices α and β to distinguish the two atoms within the ith molecule. Since it is assumed that single-particle states form an orthogonal and normalized basis with one Wannier orbital per site labeled as "i", we have

$$\left\langle w_i^\mu(\mathbf{r})\middle|w_j^\nu(\mathbf{r})\right\rangle = \delta_{ij}\delta_{\mu\nu}, \tag{10}$$

where $\mu,\nu \in \{\alpha,\beta\}$.

In this manner, each atom is labeled with the pair (i,μ) of the indices which also results in the labeling of the microscopic parameters, i.e., $t_{ij} \to t_{ij}^{\mu\nu}$ and $V_{ijkl} \to V_{ijkl}^{\mu\nu\tau\rho}$. Effectively, we consider a degenerate two-orbital system.

Functions $w_i^\mu(\mathbf{r})$ are approximated by means of the *tight-binding* approach, i.e., as a linear combination of $1s$ Slater orbitals which are defined as

$$\psi_i^\mu(\mathbf{r}) \equiv \sqrt{\frac{\zeta^3}{\pi}}e^{-\zeta|\mathbf{r}-\mathbf{R}_i^\mu|}, \tag{11}$$

where ζ becomes a single variational parameter to be adjusted in the correlated and $\mathbf{R}_i^\mu$ stands for the atomic position. In effect, the orthogonal (Wannier) functions constructing the microscopic parameters [cf. Eqs. (7a) and (7b)] are defined in the form

$$w_i(\mathbf{r}) \approx \sum_{j(i)}^{L(i)} \sum_{\mu\in\{\alpha,\beta\}} c_{j\mu}\psi_j^\mu(\mathbf{r}), \tag{12}$$

with the summation related to j extended up to the 13th coordination zone (cf. Fig. 2).The mixing coefficients $c_{j\mu}$ for a given set $\{a,R,\zeta\}$ are to fulfill condition (10) with the help of the previously elaborated procedure [17,18]. Both one- and two-electron integrals [Eqs. (7a) and (7b), respectively] are taken into account up to the 13th coordination zone, i.e., extend beyond the supercell; in this sense we include longer-range interactions than the four-molecule unit depicted in Fig. 1. Note that subscript indices in the hopping and the interaction terms in (7) are related to the positions of the atomic centers, i.e., each pair refers to the $|\mathbf{R}_i - \mathbf{R}_j|$ distance. We choose the indexing in such a manner that the coordination zone number z for $i = 0$ fulfills relation $z = j$. In accordance with our previous investigations [17], we consider only the two-electron terms with the following coupling constants:

$$V_{iiii}^{\mu\mu\mu\mu} \equiv U, \quad V_{ijij}^{\mu\nu\mu\nu} \equiv K_{ij}^{\mu\nu}, \tag{13}$$

with $\mu \neq \nu$ when $i = j$. In effect, taking into account the classical electrostatic interactions between the protons, as well as the interactions within single molecule, the total Hamiltonian describing the system is taken in the atomic units in the following form:

$$\begin{aligned}\hat{\mathcal{H}} = &\sum_{i\mu}\epsilon_i^\mu\hat{n}_i + {\sum_{ij\mu\nu\sigma}}' t_{ij}^{\mu\nu}\hat{c}_{i\mu\sigma}^\dagger\hat{c}_{j\nu\sigma} \\ &+ U\sum_{i,\mu}\hat{n}_{i\mu\uparrow}\hat{n}_{i\mu\downarrow} + \frac{1}{2}{\sum_{ij\mu\nu}}' K_{ij}^{\mu\nu}\hat{n}_{i\mu}\hat{n}_{j\nu} \\ &+ \frac{1}{2}\sum_{ij}\frac{2}{|\mathbf{R_i}-\mathbf{R_j}|},\end{aligned} \tag{14}$$

where $\epsilon_i^\mu \equiv t_{ii}^{\mu\mu}$ and $\hat{n}_{i\mu} \equiv \hat{n}_{i\mu\uparrow} + \hat{n}_{i\mu\downarrow} = \hat{c}_{i\mu\uparrow}^\dagger\hat{c}_{i\mu\uparrow} + \hat{c}_{i\mu\downarrow}^\dagger\hat{c}_{i\mu\downarrow}$. The primed summations exclude the case of concurrent $i = j$ and $\mu = \nu$. Also, we have neglected here direct exchange-interaction terms and the additional many-site terms, as they are regarded as not essential to the physics of the problem, when considering the threshold of metallicity approached from the molecular side. Note that here we consider only the square bilayer system, as the principal message of the paper is to formulate the highly nontrivial problem of proper account of electronic correlations and accompanied by them the diamagnetic molecular—quasiatomic paramagnetic transition. A detailed discussion of different (e.g., close-packed) structure is deferred to a separate analysis [25].

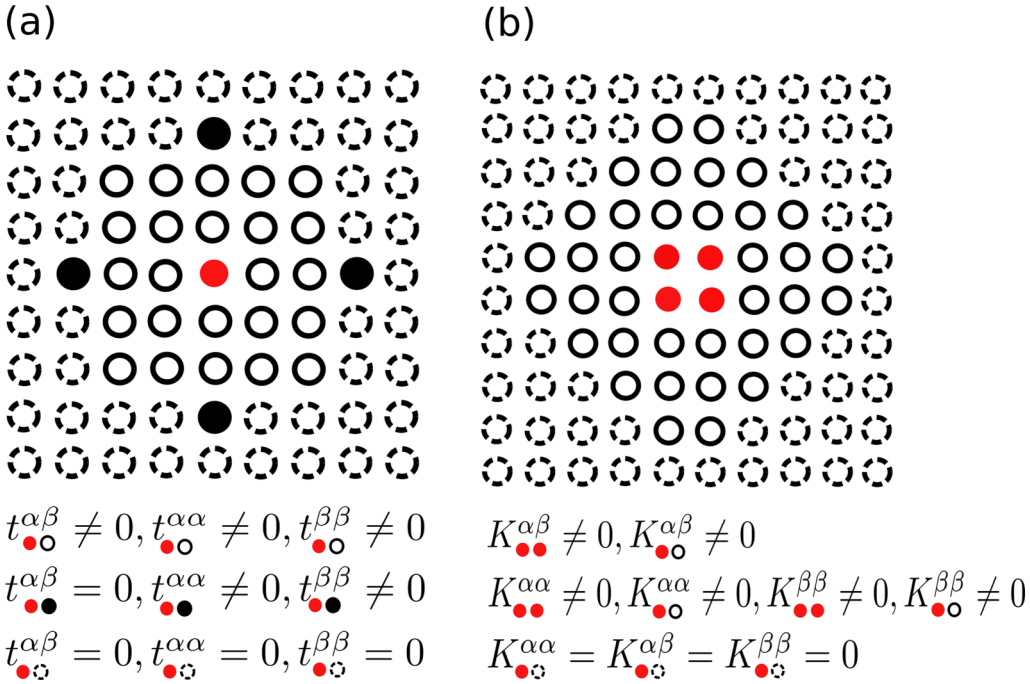

FIG. 2. Schematic representation of nonzero hoppings (a) and electron-electron interaction terms (b), taken into account in the Hamiltonian (14). The corresponding nonzero terms included are listed explicitly and represent the matrix elements between site pairs marked also as the solid or bold circles. Note that the parameters $t^{\alpha\beta} = K^{\alpha\beta} = 0$ determine the range of the corresponding dynamical processes accounted for in an exact manner.

IV. COMPUTATIONAL METHOD AND PHYSICAL RESULTS: FROM 2D MOLECULAR CRYSTAL TO QUASIATOMIC METALLIC BILAYER

A. Enthalpy and the pressure definition in two dimensions

The 2D system is studied here at temperature $T = 0$, under action of an external side force (effective pressure). However, in such a two-dimensional situation the *pressure* has to be redefined. Namely, an external homogeneous force is exerted on the 2D crystal in the planar (x-y) directions. Therefore, this situation is a 2D analog of the action of hydrostatic pressure onto a three-dimensional system. The elementary volume of 2D crystal is simply

$$v_{2D} \equiv a^2, \tag{15}$$

and thus the pressure in the present case is

$$p \equiv p_{2D} \equiv \frac{f}{a}, \tag{16}$$

where f is the force per "*unit cell*" exerted homogeneously on the system in the planar directions. By taking this definition of pressure we have the usual definition of the work part of the internal energy (or the enthalpy) as $fa = pv_{2D}$. Note that an *infinite* nature of the system is considered here preserved by means of applying PBC. Finally, a proper function of state, which in this case is 2D enthalpy per molecule can be defined as

$$h \equiv \frac{E(a,R)}{N} + p_{2D}v_{2D}, \tag{17}$$

where $E(a,R)$ is the ground state energy for given structural parameters a and R (cf. Fig. 1). We scan the space (a,R) of the parameters to obtain the energy landscape of $E(a,R)$. Note that the meaning of f arises from the notion that the enthalpy should be defined as an extensive function of the system volume $v_{2D}N$, where N is the number of molecules in the system. Also, as an outcome of our approach, we obtain evolution of the system as a function of the applied force as the only independent variable, i.e., $E(a,R) \equiv E(a(f),R(f))$. In this manner, the theory is fully microscopic, as all the microscopic parameters of the Hamiltonian (14), as well as a and R, are determined explicitly, within our EDABI procedure.

B. Computational details

The whole procedure is composed of the three stages: (i) selection and orthogonalization of the starting trial basis $\{w_i^\mu(\mathbf{r})\}$, (ii) calculation of integrals $t_{ij}^{\mu\nu}$ and $K_{ij}^{\mu\nu}$, and (iii) diagonalization of Hamiltonian matrix and concomitant minimization of the ground state energy with respect to $\{\lambda\}$.

The orthogonal single particle basis is obtained (i) in terms of the numerical solution of the bilinear set of equation (10) with the desired accuracy (10^{-6} in our case is assumed as sufficient). Step (ii) is also performed numerically by means of the previously elaborated method [18]. Each of the Slater $1s$ orbitals, which are the *building blocks* of $\{w_i^\mu(\mathbf{r})\}$ functions [see Eq. (12)], are approximated by three Gaussian functions that simplify the calculation of the two-electron integrals composing $\{V_{ijkl}^{\mu\nu}\}$ [17,18]. Note also that according to the spatial *cutoff* assumed for the repulsive Coulomb interactions, there are $23 + 1 = 24$ (intersite plus one intrasite, respectively) $K_{ij}^{\mu\nu}$ integrals to be computed, carried out each time when the variational parameter ζ is updated during the minimization procedure. This stage is the most time consuming in the whole procedure. The step (iii), i.e., the Hamiltonian matrix

diagonalization, is performed for the moderately sized matrix (12870 × 12870), and results from the assumed model, i.e., that with the half filling for the eight-site system. The periodic booundary conditions (PBC) are imposed in the standard manner by means of inclusion of *up-to-cutoff* terms in the Hamiltonian matrix (cf. Fig. 2) which is diagonalized subsequently with the help of the Lanczos algorithm. The diagonalization of (14) results thus in obtaining the trial value of the trial ground state energy $E_G(\zeta)$. The latter is minimized with respect to ζ by means of numerical procedure devoted for a single variable function numerical scheme (e.g., *Brent*, as in this case or *golden section search*), implemented within the *Gnu Scientific Library* (GSL) used by us in this context. The typical numerical accuracy of the energy evaluation is 10^{-4} Ry. As the phase transition to the quasiatomic phase is of the first-order nature, such accuracy is sufficient as we can trace the evolution of the involved enthalpies in a systematic manner, as a function of applied pressure.

C. Discontinuous $H_2 \rightarrow 2H$ transition and its overall characteristics

We start our discussion with the remark that the solid hydrogen dissociation from molecular to the quasiatomic state, and associated with it metallization, represents one of the fundamental transitions in Nature, as it involves one of the simplest condensed systems in which the electronic correlations play a decisive role, as we discuss next. In Fig. 3 we present exemplary results for the ground-state energy versus the bond length R for the four selected values of the lattice parameter a. With the decreasing a, the molecular bond length evolves from the value $R \ll a$ at ambient pressure to that close to a. Such a changeover speaks directly about the transition from molecular to quasiatomic configuration. The detailed character of the transformation is shown in Fig. 4, where we have displayed the enthalpies of two molecular ($R \ll a$) phases and the atomic one ($R \sim a$) as a function of applied pressure. Two discontinuous (first-order) phase transitions are seen at the critical pressures $p_{c1} \sim 0.1102\ \mathrm{Ry}/a_0^2$

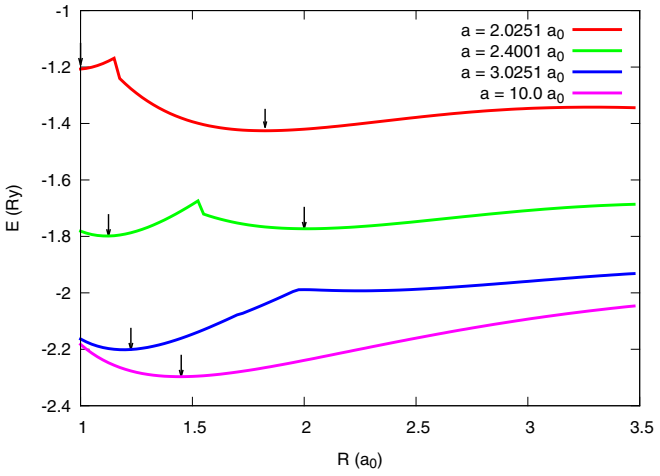

FIG. 3. Ground-state energy per molecule as a function of the bond length (intramolecular distance) R for four selected values of the lattice parameter a. The minima are marked by the vertical arrows.

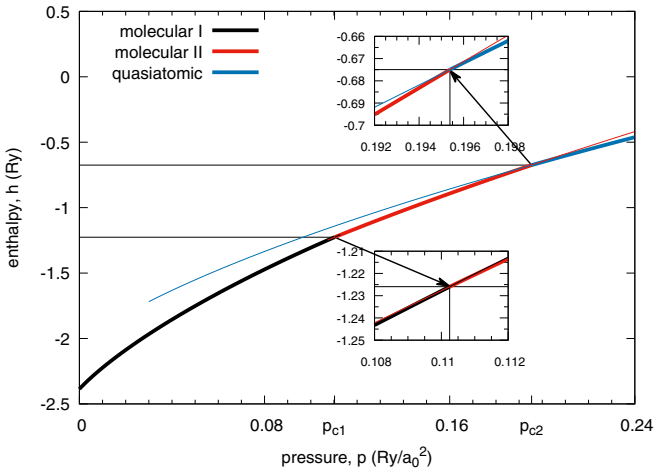

FIG. 4. Enthalpy (per molecule) versus pressure p. At lower pressure, two molecular phases are stable; the transition to the *quasiatomic* phase occurs at $p_{c2} \sim 0.1954\ \mathrm{Ry}/a_0^2$, as marked. $E_B(p=0) = -2.3858$ Ry, $R_{\mathrm{eff}}(p=0) = 1.4031a_0$, and $a(p=0) = 4.3371a_0$. Thin lines extrapolate the enthalpies of the particular phases beyond the regime of their stability. Insets show some detail on the transitions. For details, see main text.

and $p_{c2} \sim 0.1954\ \mathrm{Ry}/a_0^2$, respectively, where a_0 is the Bohr radius. Note that at $p = 0$ the equilibrium values of the binding energy and the bond length are $E_B = -2.3858$ Ry and $R = 1.4031a_0 = 0.7425$ Å, respectively. These values can be compared with those for H_2 molecule: $E_B = -2.295$ Ry and $R = 0.74144$ Å [1]. So the solid molecular bilayer is stable against the dissociation into individual molecules and the bond length in the former case is larger by 0.14%. This result provides *a crucial test of our method* reliability when applied to the multimolecular systems. Obviously, the values of E_B at $p = 0$ prove only that the solid molecular phase is stable for $p < p_{c2}$ from the electronic point of view, as we have not included as yet the zero-point motion. Those will be estimated later. The application of pressure will help additionally to stabilize it.

In Fig. 5 we plot the equilibrium lattice parameter (in units of $a_0 \approx 0.53$ Å) versus pressure and observe a discontinuous lattice contraction for both the transitions by about 3% and 9% at the pressures p_{c1} and p_{c2}, respectively. In an analogous manner, the bond length versus pressure jumps from the equilibrium value $R_{\mathrm{eff}} \ll a$ to $R_{\mathrm{eff}} \sim a$ at the critical pressure p_{c2}, as shown in Fig. 6. Hence the transitions are strongly discontinuous between each of the two pair of three stable phases. The phase diagram for the scanned space of (a, R) is composed of three phases. Those referring to $p \leqslant p_{c1}$ and $p_{c1} \geqslant p \leqslant p_{c2}$ we recognize as both being of a *molecular* kind and label them as phases I and II, respectively, while the phase referring to $p \geqslant p_{c2}$ is the *quasiatomic* one. This distinction may seem at this stage as somewhat arbitrary and is legitimate only by making the observation that the ratio $a/R \geqslant 2$ for stable phase referring to $p \leqslant p_{c2}$ and $a/R \approx 1$ for $p \geqslant p_{c2}$. However, a more convincing argument which originates from the diversity of electronic properties for both of the two groups of phases is provided in the next subsection. As supplementary information we have plotted in Fig. 7 the

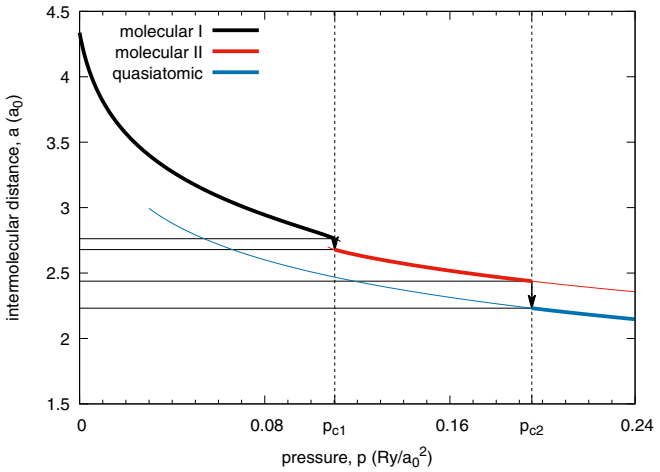

FIG. 5. Intermolecular distance (lattice parameter) a for 2D bilayer crystal as a function of pressure p. The transitions are clearly of discontinuous (first-order) nature at temperature $T = 0$. Note a spectacular decrease of lattice parameter by 8.47% (corresponding to 16.22% volume decrease) at the transition (p_{c2}) from molecular to quasiatomic phase. The thin lines denote the lattice parameter of the phases in the regime, where they are not of the lowest enthalpy. The arrows mark the jump of the intermolecular distance at the transitions with the increasing pressure.

inverse Bohr radius ζ^{-1} versus p for the Slater functions composing the Wannier functions. The jumps take place by $\sim$27% at p_{c1} and by $\sim$30% at p_{c2}, so the wave-functions site is strongly altered at both the transitions. Note that ζ^{-1} value in the H_2 phase is close to that for the hydrogen atom (within $\sim$3%) even though the actual value in the quasiatomic solid phase is only about 75% of the single-atom value. This last result is certainly counterintuitive. Interelectronic correlations,

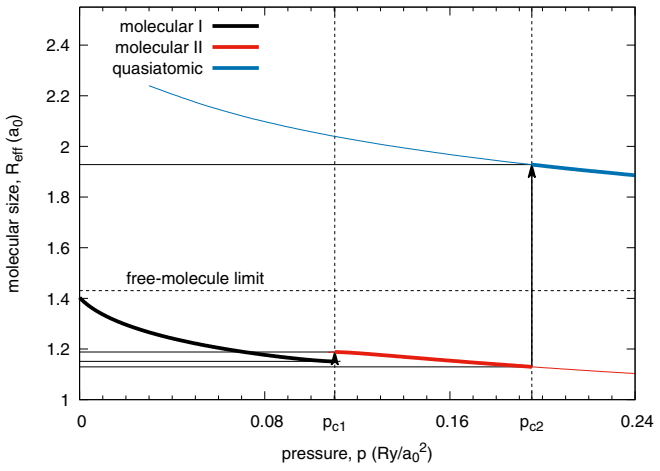

FIG. 6. Intramolecular distance (bond length) R as a function of pressure p. An abrupt change by 70.69% at the transition from molecular to quasiatomic state (at p_{c2}) is clearly visible. The spectacular increase of the optimized bond length $R = R_{\text{eff}}$ at p_{c2} is taking place towards quasiatomicity (cf. Fig. 5). Only a small difference between R_{eff} in both of the molecular phases (3.21%—close to p_{c1}) is observed. The arrows mark the interatomic distance jump at p_{c1} and p_{c2} when increasing p.

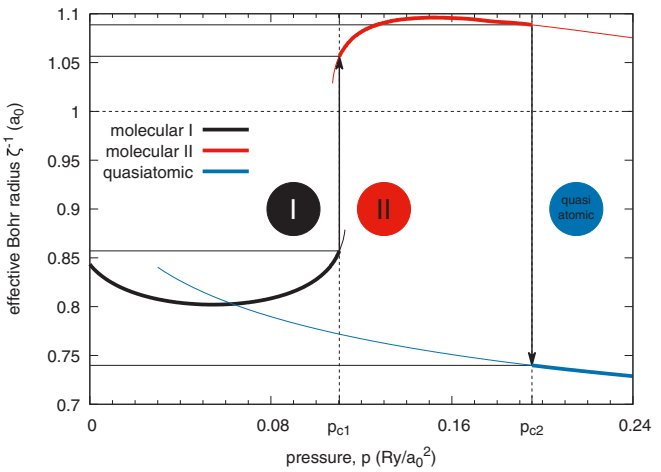

FIG. 7. Effective Bohr radius $1/\zeta$ of the renormalized Slater orbitals composing the Wannier functions for a 2D system, as a function of pressure p. The atomic function size changes by 27.02% at the transition to the molecular phase II and by 29.97% at the transition to the quasiatomic (metallic) state. The arrows mark the Slater-orbital size jumps when increasing p.

induced by the interatomic repulsive interactions, reduce the effective Bohr radius by over 17% in the molecular phase II.

D. Principal electronic characteristics of the Mott-Hubbard $H_2 \rightarrow 2H$ transition

For the sake of completeness, we list in Table I principal parameters of the three states calculated at the critical pressures. Particularly interesting are $t_{00}^{\alpha\beta}$ and $t_{01}^{\alpha\alpha}$, the intra- and intermolecular hopping integrals, since they change remarkably at the transition. The same concerns the values of the Hubbard gap $U - W$ (with the bare bandwidth W calculated in Appendix A) and the U/W ratio (cf. Figs. 8 and 9, respectively). The last characteristic is particularly important since at the transition at p_{c2} it jumps from $U/W = 1.3112$ (>1) in the molecular state to the value 0.6000 (<1) and represents a typical trend for the Mott-Hubbard transition, albeit this time from an originally diamagnetic molecular insulator to a paramagnetic metal. The negative value of the Hubbard gap means that the two lowest bands overlap appreciably and therefore the system can be regarded as metallic. Also, there is a principal difference between the present approach and the canonical treatments [13,22,23] of the Hubbard model, as here the value of the bandwidth changes at the transition and, in effect, the U/W ratio is not changing in a continuous manner, as one would have in all the parametrized-model considerations [26–28]. Also, a relatively large value of the intersite Coulomb interactions may mean that either the spin (SDW) or the charge (CDW) -density-wave states become a stable phase on the quasiatomic side, at least in the low-temperature range. This topic should be analyzed separately, as it is more complicated than the present analysis. Such an analysis would allow for differentiating in detail between the present transition from the diamagnetic insulator and the canonical Mott-Hubbard transition which takes place from an antiferromagnetic (Mott) insulator to

TABLE I. Values of the principal parameters at both the transition pressures and on both sides of those discontinuous transitions. For explanation of notation see Fig. 2 and main text. The numerical accuracy is at the level of the last digit.

	p (Ry/a_0^2)	a (a_0)	$R_{\rm eff}$ (a_0)	ζ (a_0^{-1})	U (Ry)	$K_{00}^{\alpha\beta}$ (Ry)	$K_{01}^{\alpha\alpha}$ (Ry)	$t_{00}^{\alpha\beta}$ (Ry)	$t_{01}^{\alpha\alpha}$ (Ry)
Molecular I	0.1102	2.7626	1.1511	1.1667	1.8268	1.0725	0.7173	−1.1985	−0.1933
Molecular II	0.1102	2.6791	1.1881	0.9466	1.6751	0.9847	0.7289	−1.1177	−0.1422
Molecular II	0.1954	2.4378	1.1296	0.9186	1.7486	1.0244	0.7945	−1.2456	−0.1596
Quasiatomic	0.1954	2.2313	1.9281	1.3516	2.0392	0.9380	0.8760	−0.7660	−0.3884

either SDW or a paramagnetic correlated metal. Also, as said above, the Mott-Hubbard transition is analyzed customarily as a function of U/W ratio changing continuously [26–29]. As our results show explicitly this is not the case, when the renormalization (readjustment) of the orbitals is taken into account in the correlated state. In this respect, our approach is fully microscopic (parameter free).

The transition can be elaborated further by calculating directly the intramolecular ($\langle\hat{c}_{0\alpha}^{\dagger}\hat{c}_{0\beta}\rangle$) and the intermolecular hopping correlation functions, both displayed in Fig. 10. Note that the value of correlation function $\langle\hat{c}_{i\mu}^{\dagger}\hat{c}_{jv}\rangle \equiv \sum_{\sigma}\langle\hat{c}_{i\mu\sigma}^{\dagger}\hat{c}_{jv\sigma}\rangle$ reaches the value $\frac{1}{2}$ in the quasiatomic phase which we identify with the system metallicity. This is because this value reaches an amazing value $n(1-\frac{n}{2}) = \frac{1}{2}$ for $n = 1$ electrons per atom, characteristic of the uncorrelated lattice fermionic gas [30]. On the contrary, the value of $\langle\hat{c}_{0\alpha}^{\dagger}\hat{c}_{1\alpha}\rangle$ in the molecular phases is close to zero, whereas $\langle\hat{c}_{0\alpha}^{\dagger}\hat{c}_{0\beta}\rangle \approx 1$ then, both characteristic of a molecular insulator. It is amazing that such spectacular switching from an almost ideal insulator to an almost ideal fermionic gas takes place in this situation. The situation described here is in accord with an old argument of Mott [31] that switching to a metallic state can take place only in a discontinuous manner as a creation of a small number of carriers in a nominally insulating state would largely increase the system energy due to the lack of screening of the long-range repulsive Coulomb interaction between them. Here, this argument is fully qualified and includes also the Hubbard argument [21] in the same manner. In effect, the solid hydrogen may be indeed regarded as the model example of the transition from a correlated, albeit diamagnetic insulator to a moderately/weakly correlated paramagnetic metal, if we only account properly for its original molecular H_2 structure in a solid at ambient pressure, and subsequently the renormalization of both the molecular and the atomic (Slater) orbitals by the interelectronic correlations. The values of the lattice and microscopic parameters at the transitions are listed in Table I.

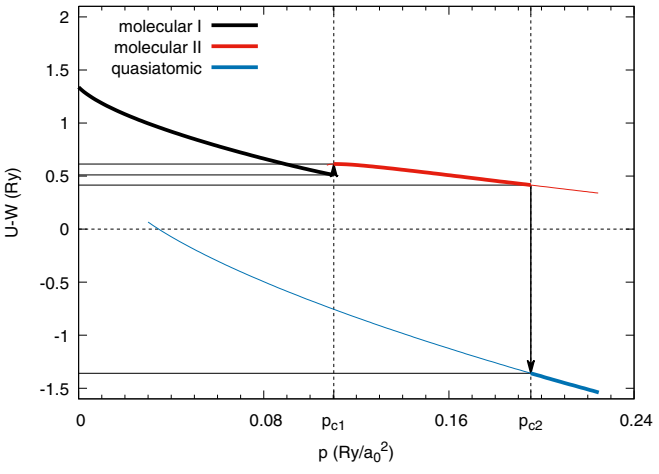

FIG. 8. Estimate of the Hubbard gap, $U - W$, with the bare bandwidth W computed for the single-electron part of Hamiltonian (14) as a function of p in the molecular and quasiatomic correlated states. The bandwidth changes radically at p_{c2}. The negative gap value means that the two bands overlap and hence the system is in metallic state (for a detailed discussion, see main text). The arrows mark the sequence of jumps with the increasing pressure.

E. Electron density evolution and renormalized single-particle band characteristics in the correlated state

To complete our picture of the metallization we have also determined the electron densities $n(\mathbf{r}) \equiv \langle\hat{\Psi}^{\dagger}(\mathbf{r})\hat{\Psi}(\mathbf{r})\rangle$ in the many-particle states; those are displayed in Figs. 11 and 12, in both the molecular and the quasiatomic states. The nature of the states does not alter qualitatively in Fig. 11;

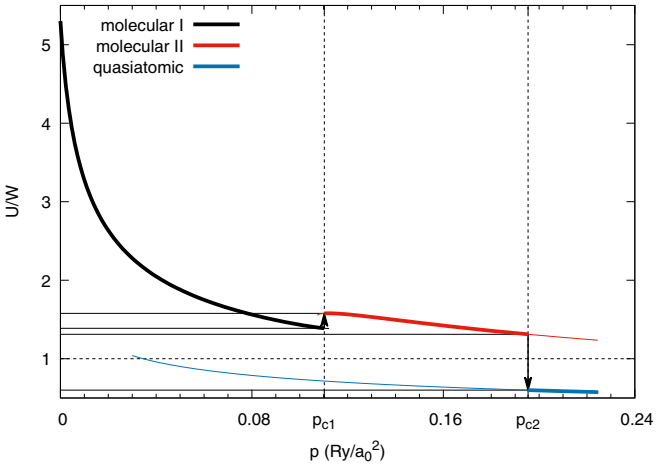

FIG. 9. Ratio between the intra-atomic (Hubbard) repulsion amplitude U and the lower-bandwidth W in the correlated state, as a function of p. Both quantities are calculated for the renormalized orbitals composing the Wannier functions. At the critical pressures the ratio jumps: from the value 1.3880 to 1.5778 at p_{c1} (at the transition between the two molecular phases), and from 1.3112 to 0.6000 at p_{c2}, i.e., at the transition to the quasiatomic phase. The latter defines the Mott-Hubbard-type transition to a moderately correlated state. Close to the transition, even in the molecular phases the value of the bare bandwidth W is not decisively smaller than U. The arrows mark the jumps when increasing the pressure.

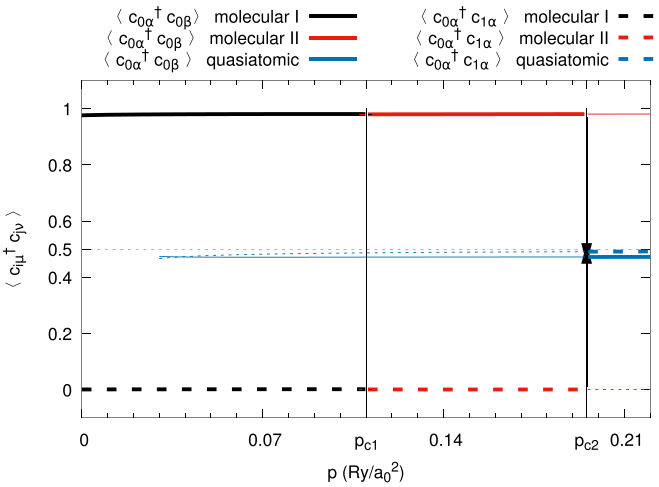

FIG. 10. Principal hopping correlation functions $\langle \hat{c}^{\dagger}_{i\mu}\hat{c}_{j\nu}\rangle$ versus pressure p. $\langle \hat{c}^{\dagger}_{0\alpha}\hat{c}_{0\beta}\rangle$ corresponds to the intramolecular hopping and $\langle \hat{c}^{\dagger}_{0\alpha}\hat{c}_{1\alpha}\rangle$ to the intermolecular one. Note that some of the straight lines coincide. Note that whereas for the molecular crystal the dominant hopping is $\langle \hat{c}^{\dagger}_{0\alpha}\hat{c}_{0\beta}\rangle = 1$ and the remaining one is almost equal to zero, for the quasiatomic phase the presented correlation functions in the metallic state are almost equal to those for free electrons, i.e., $\approx 1/2$. Such a behavior provides us with a clear sign of both quasiatomic nature and metallic character of the highest-pressure state, as the renormalized hoppings are practically the same and equal to $\frac{1}{2}$.

they represent indeed the two molecular states, differing only by the bond length, etc. On the contrary, the nature of the molecular–quasiatomic transition is very clear, since the density shown in Fig. 12(b) splits with respect to (a) into two disjoint regions representing well separated states of atoms. The latter states are called quasiatomic because their size (cf. Fig. 7) differs remarkably with respect to that of an isolated H atom.

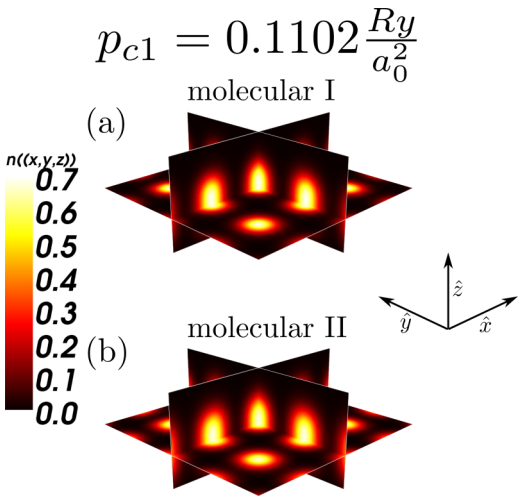

FIG. 11. Electronic density $n(\mathbf{r})$ in 3D near the molecular I (a) $\rightarrow$ molecular II (b) transition at $p_{c1} = 0.1102$ Ry a_0^{-2}. The ellipsoidal character of density is a signature of H_2 molecular states with the symmetric character (with respect to the molecule center of mass) of its spatial distribution.

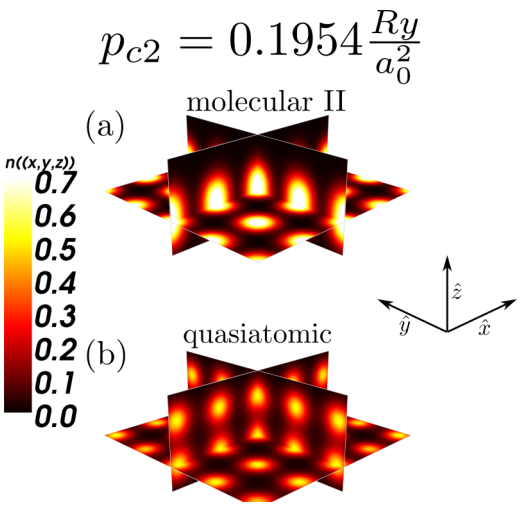

FIG. 12. Electronic density $n(\mathbf{r})$ in 3D near the molecular II (a) $\rightarrow$ quasiatomic (b) transition ($p_{c2} = 0.1954$ Ry a_0^{-2}). Note a clear changeover from the molecular ellipsoidal (top) to the quasiatomic (spherical) configuration shape of the density, characteristic for symmetric-in-space molecular states and quasiatomic nature of the single-particle states, respectively. Also, the electronic-density profiles illustrate directly the character of the Mott-Hubbard transition at $p = p_{c2}$.

The above evolution of electron density for molecules/atoms placed in the milieu of all other particles is supplemented with the selected relevant parameters displayed in Table II, where we list the values at the consecutive transitions (marked withe subscript c in each case): $p = p_c$, $a = a_c$, $R = R_{\mathrm{eff},c}$, as well as provide the critical values of the Hubbard ration $(U/W)_c \sim 1$ and of the Mott criterion "$n_c^{1/D} a_B \sim 0.22$", here adopted to the two dimensional ($D = 2$) case, for which the effective Bohr radius is $a_B \equiv \zeta_c^{-1}$ and the particle density $n_c = \frac{1}{a_c^2}$. Those three quantities are listed in the last two columns. It is amazing that those two sets of values, introduced via a rough estimates, are not far off from the standard estimates [12] at the transition to the quasiatomic state.

In Figs. 13(a) and 13(b) we have determined the two lowest bare-bands dispersion relations calculated with the renormalized hopping parameters and at the transition from the molecular phase I to II, as well as in Figs. 13(c) and 13(d) at the transition from phase II to the quasiatomic phase. As the interactions are not included in those calculations, we do not have the Hubbard-subband structure at the transition from I to II. Nevertheless, since then $U/W > 1.5$, the structure represents that of an insulators, whereas the quasiatomic phase is metallic, as there is an appreciable band overlap is that state and the correlations are moderate to weak ($U/W \sim 0.5$). The phases I and II are both insulating; they differ only by different values of the microscopic parameters. It is tempting to suggest that while the phase I is diamagnetic, the phase II may be insulating and (antiferro)magnetic. However, this point requires a separate analysis.

To provide illustrative evidence for the existence of two distinct molecular phases, the enthalpy minima corresponding to them at those two transitions have been visualized in

TABLE II. Values of the equilibrium lattice parameters, as well as the Mott-Hubbard and Mott criteria at both transitions.

	p_c (Ry/a_0^2)	a_c (a_0)	$R_{\mathrm{eff},c}$ (a_0)	ζ_c^{-1} (a_0)	$(U/W)_c$	$(\zeta_c a_c)^{-1}$
Molecular I	0.1102	2.7626	1.1511	0.8571	1.3870	0.3103
Molecular II	0.1102	2.6791	1.1881	1.0564	1.5778	0.3943
Molecular II	0.1954	2.4378	1.1296	1.0887	1.3112	0.4466
Quasiatomic	0.1954	2.2313	1.9281	0.7398	0.6000	0.3316

Figs. 14(a) and 14(b). We see that even in 2D there are two states and this circumstance may be regarded as a precursory effect for a number of such phases appearing in experiment on 3D systems [3,8].

To illustrate the changes in the single-particle functions at the transitions, we have drawn the Wannier functions at the I→II- (cf. Fig. 15) and II→quasiatomic-state (cf. Fig. 16) transitions along in-plane [x (a)] and molecular [z (b)] directions. The two equilibrium lattice and bond parameters have been supplied in each of the figures. Their evolution reflects perfectly the trend of the Slater-orbital size (ζ^{-1}) jumps shown in Fig. 7. It is amazing that they look more atomiclike in the last, metallic phase. However, the situation is not so simple, since at the same time the lattice parameter a decreases appreciably in a discontinuous manner at the same time and therefore the change of Hamiltonian parameters is also influenced by that. Nonetheless, the bond-length changes are most important (cf. Fig. 14).

Concluding this section, the results presented in Figs. 8 to 16 provide unequivocal evidence for the molecular to quasiatomic phase transition at the critical pressure $p_{c2} = 0.1954$ Ry/a_0^2. Obviously, further evidence of metallicity in the latter phase would require a direct calculation of the electric conductivity. Namely, it would require an extension of the present approach to nonzero temperature, as here the conductivity σ_c at $T = 0$ would take the values $\sigma_c = 0$ in the molecular phases and $\sigma_c = \infty$ in the metallic ground state. However, the gap closure at the II →quasiatomic discontinuous phase transition

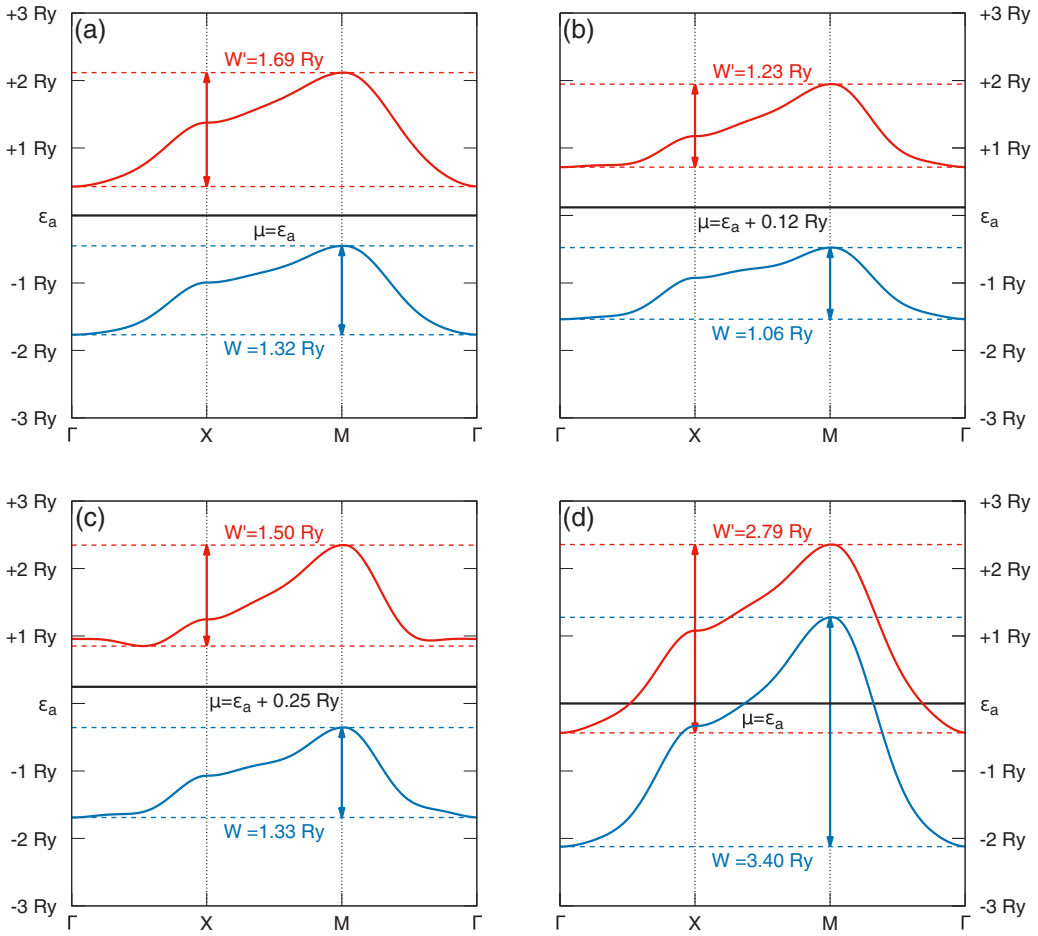

FIG. 13. (a),(b) Dispersion relations for bare bands at the molecular I → molecular II transition ($p_{c1} = 0.1102$ Ry/a_0^2). (c),(d) The same at the molecular II → quasiatomic transition ($p_{c2} = 0.1954$ Ry/a_0^2). One expects that the lowest band in (a)–(c) will split additionally into the Hubbard subbands in those states as then $U/W > 1.5$, whereas in the state (d) they will overlap as the $U/W \approx 0.5$, i.e., the system eventually becomes a moderately correlated metal.

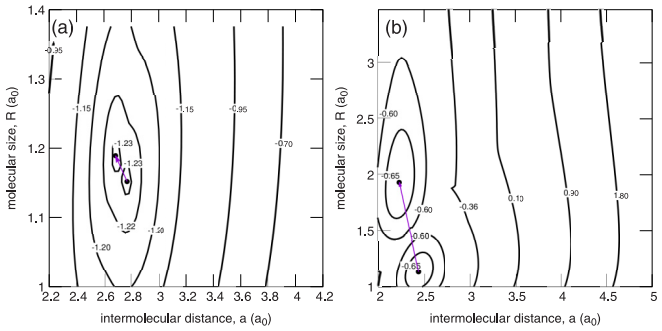

FIG. 14. Enthalpy isolines on the plane a-R at the border between I and II states (a) and at the II-quasiatomic border (b). The points mark the minima with the arrow connecting them as a guide to the eye. Note that both transitions involve primarily a radical change in the effective molecule size $R_{\rm eff}$.

(cf. Fig. 13) provides a clear sign of metallicity in the latter phase.

V. OUTLOOK

A. Brief summary and zero-point motion of atoms

Let us summarize first our effort here. We have discussed the metallization of a 2D stack of molecular hydrogen within the EDABI method. The fully microscopic model relies on an exact diagonalization of the extended Hubbard Hamiltonian describing the dynamic processes within a supercell containing $4H_2$ molecules; this cluster is subsequently repeated periodically in both planar directions, with additional inclusion of hopping and interelectronic interactions extending beyond the supercell (cf. Fig. 2). In this respect, our approach represents a version of the coupled-cluster approach [32]. Furthermore, at each step of the iterative diagonalization procedure by Lanczos method we readjust the single-particle (Wannier) wave function until a fully microscopic ground-state energy configuration is reached. Therefore, the input parameters are solely the initial structure of the molecules (cf. Fig. 1) and the finite single-particle basis, limited here to $1s$-type Wannier states. As a result, we obtain the principal characteristics such as the lattice constant, the effective bond length, renormalized band structure and single-particle wave functions, and the ground-state enthalpy, all as a function of applied force. But first and foremost, we obtain the sequence of discontinuous phase transitions and, in particular, the insulator–metal transition from the H_2 insulator to H metal. The atomization process is illustrated directly in Figs. 12(a) and 12(b), where the many-particle electron-density profiles have been drawn. All this provides the evidence that the hydrogen metallization represents a transition of the Mott-Hubbard type, though the starting material at ambient pressure is a diamagnetic (not antiferromagnetic) insulator. Hence our approach represents an essential extension of the concept of the canonical Mott-Hubbard transition. Additionally, the microscopic parameters of the extended Hubbard Hamiltonian have been calculated within the scheme.

Our analysis would be complete if we supplemented the present work with the study of stability of the assumed protonic lattice in the metallic state. In other words, a separate question can be asked if the metallization is not associated with the transition to a liquid proton-electron plasma [4,33–36], though the corresponding transition in the liquid state is also observed [37]. The latest experimental results [6] support the view taken here that the lattice survives the strong first-order transitions (see, however, Ref. [38]). The stability of the lattice can be justified by two features of our results. First, we have shown that at the transition the electron orbit shrinks remarkably (cf. Figs. 7 and 16), screening the charges on a short-distance scale and thus diminishing the repulsive energy. Second, in Appendix B we have estimated the amplitude and the energy contribution of the zero-point motion in the harmonic approximation [20,39] and both in the inter- and intramolecular directions. The inclusion of the zero-point motion can change only slightly the transition points without changing the overall features of our results. Note that the ZPM energy does not exceed 1% of the total enthalpy value (cf. Fig. 4), but up to about 4% of the ground-state-energy value.

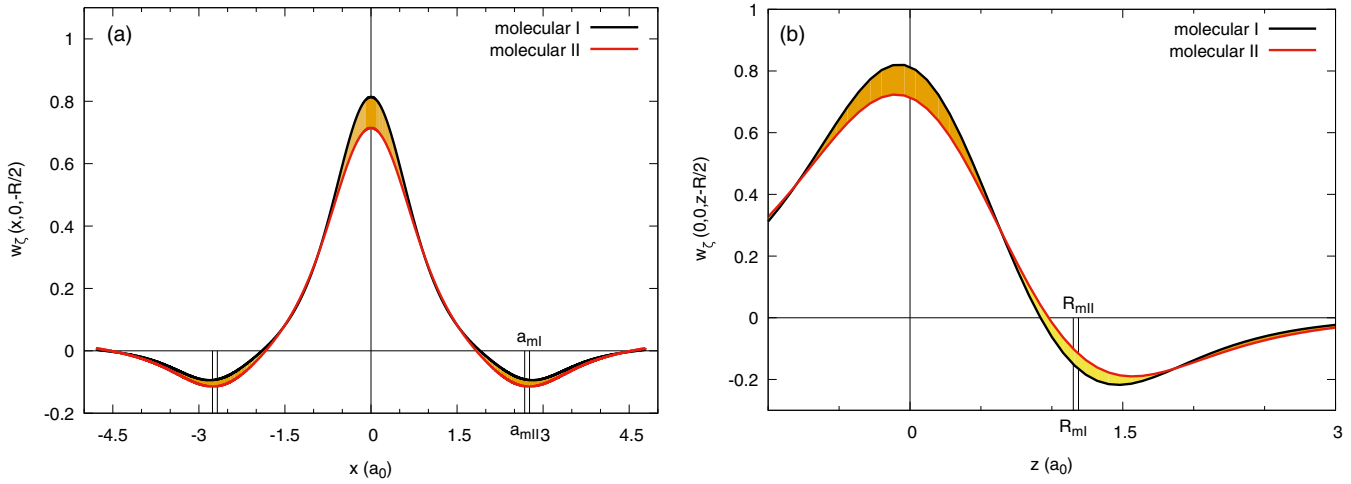

FIG. 15. Single-electron wave functions $w_0^\beta(\mathbf{r}=(x,0,-R/2))$, in the planar direction (a) and $w_0^\beta(\mathbf{r}=(0,0,z-R/2))$ (b) (along the molecule, z direction) in the molecular phases I [$a=2.76261(a_0)$, $R_{\rm eff}=1.1511(a_0)$, $\zeta=0.8571(a_0^{-1})$] and II [$a=2.67911(a_0)$, $R_{\rm eff}=1.1881(a_0)$, $\zeta=1.0564(a_0^{-1})$] near the transition (at $p_{c1}=0.1102{\rm Ry}/a_0^2$).

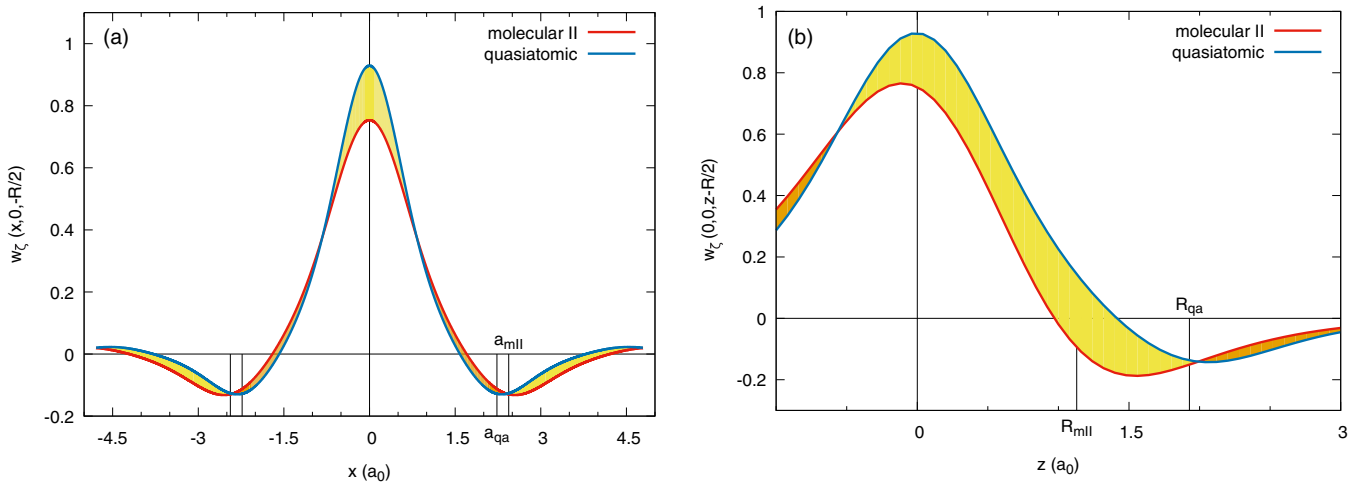

FIG. 16. Single-electron wave functions $w_0^\beta(\mathbf{r} = (x,0,-R/2))$ (a) and $w_0^\beta(\mathbf{r} = (0,0,z-R/2))$ (b) (along the z direction) in molecular phase II [$a = 2.43783(a_0)$, $R = 1.1296(a_0)$, $\zeta = 1.0887(a_0^{-1})$] and in the quasiatomic phase [$a = 2.23133(a_0)$, $R = 1.9281(a_0)$, $\zeta = 0.7398(a_0^{-1})$] near the transition (at $p_{c2} = 0.1954$ Ry$/a_0^2$). Note the shrinking in the quasiatomic phase.

B. Relation to other works

Our approach relies on (i) implementing a combined first- and second-quantization scheme which allows for a full *ab initio* analysis of the correlated state without the appearance of the notorious double-counting problem, (ii) determining the renormalized Wannier orbitals which supplement the whole picture qualitatively with respect to that obtained within the parametrized models, and (iii) applying the concepts of the Mott-Hubbard transition to the canonical solid hydrogen system with $1s$ orbitals. The transition is accompanied by a simultaneous two-step transition from the correlated diamagnetic molecular insulator to the two-dimensional metal as a function of applied pressure. The inclusion of long-range Coulomb interaction should also be noted. The question remains as to whether such a bilayer system can be realized experimentally by, e.g., covering a substrate with a plane of such stacked H_2 molecules, with the substrates of variable lattice parameter emulating the pressure applied to the system edges. Such an experiment could provide a direct realization of a bilayer crystal in a metallic state. In this case of a bilayer deposited on the substrate one would have to account also for the dynamics of the protons and electrons in the presence of external trapping (surface) potential which, if sufficiently strong, would suppress their zero-point vibrations.

This work is by no means complete. Even though the present planar square structure is stable at $p = 0$ against dissociation into gas of molecules, other (close-packed) structures such as triangular should also be considered. However, in the case of the triangular lattice the frustration effects must be considered carefully and hence the exchange interactions included in the starting Hamiltonian. In effect, such an effort requires a separate analysis [25]. The principal features of two-step metallization appear also there, so the "Mottness" of the system seems to be independent of the starting crystal structure.

Other theoretical works involve among others recent diffusion quantum Monte Carlo simulations [8,40] and advanced DFT methods [41,42]. Both methods predict the metallization for pressures in the range 400–500 GPa in the three-dimensional case. Here we show that the transition in the bilayer case is of the Mott-Hubbard type. The same type of the transition has been shown to exist in a one-dimensional case [17] for the molecular ladder. Therefore, we expect that the same type of results can be expected in the 3D case, but a proof of that hypothesis requires a more involved approach and should employ the incorporation of the Monte Carlo methods into our scheme. The reason why our results are to a certain degree independent of the lattice dimensionality is the fact that we include long-range Coulomb interactions between the electrons which makes the results look more like those of mean field theory of those correlated fermion systems, results of which are only weakly dependent on the system dimensionality.

At the end we would like to note about a very recent extensive review on many-electron states in atomic hydrogen chain [43]. Here we consider a two-dimensional situation in this context and include a fundamental question of atomization of a bilayer of hydrogen molecules. The present situation is also reflected in the case of a hydrogen ladder dissociating into two linear chains [17].

C. Concluding remarks

So far we have analyzed the normal states only. As our bilayer metallic phase represents a moderate correlated system we can treat it as a bilayer system with correlation-driven pairing, analogous to our recent approach of the cuprates within the extended Hubbard model [44–46]. However, the situation is not that simple as here the electron-lattice interactions can be quite strong, as one can see already on the H_2 and $(H_2)_2$ examples [39]. In effect, both the correlation and electron-lattice parts should be treated on equal footing. In that case, one can estimate their relative contributions to the superconducting critical temperature and in such a manner complement the estimates based purely on the electron-lattice contribution [42,47,48]. We should be able to see progress along these lines in the near future.

ACKNOWLEDGMENTS

The work was financially supported by the Narodowe Centrum Nauki (NCN) through Grant No. DEC-2012/04/A/ST3/00342. The computations have been performed in part on the supercomputer TERA-ACMiN located at AGH University of Science and Technology and partly on the supercomputer EDABI located at the Jagiellonian University.

APPENDIX A: BARE BANDWIDTH W OF THE ELECTRONS IN THE CORRELATED STATE

To compute U/W ratio, the *bandwidth* W can be obtained from diagonalization of the single-electron part of Hamiltonian (14), i.e.,

$$\hat{\mathcal{H}} = \sum_{i\mu\sigma} \epsilon_i^{\mu} \hat{n}_{i\sigma} + {\sum_{ij\mu\nu\sigma}}' t_{ij}^{\mu\nu} \hat{c}_{i\mu,\sigma}^{\dagger} \hat{c}_{j\nu,\sigma}. \tag{A1}$$

In accordance with the translational invariance of the system in the x-y plane, Eq. (A1) can be rewritten in the momentum ($\mathbf{k}$) representation in the form

$$\begin{aligned}\hat{\mathcal{H}} &= \sum_{\mathbf{k}\mu\sigma} \epsilon^{\mu} \hat{n}_{\mathbf{k}\sigma} + {\sum_{\mathbf{k}\mu\nu\sigma}}' \hat{c}_{\mathbf{k}\mu,\sigma}^{\dagger} \hat{c}_{\mathbf{k}\nu,\sigma} \sum_l t_{p(l,\mu)q(l,\nu)}^{\mu\nu} \exp\left(-i\mathbf{k}\cdot\mathbf{r}_l^{\mu\nu}\right) \\ &= \sum_{\mathbf{k}\mu} \epsilon^{\mu} \hat{n}_{\mathbf{k}} + {\sum_{\mathbf{k}\mu\nu\sigma}}' \hat{c}_{\mathbf{k}\mu,\sigma}^{\dagger} \hat{c}_{\mathbf{k}\nu,\sigma} \sum_l Z_{\mathbf{k}}^{\mu\nu},\end{aligned} \tag{A2}$$

where primed summation refers to $\mu \neq \nu$ and index l enumerates molecules in the assumed neighborhood, i.e., $\mathbf{r}_l^{\mu\nu} = \mathbf{R}_0^{\mu} - \mathbf{R}_l^{\nu}$. The functions $p(l,\mu)$ and $q(l,\nu)$ map l,μ,ν to proper indexing of the hoppings. Note that one may select $\mathbf{k} = (\frac{2\pi n}{a_x}, \frac{2\pi m}{a_y}) = (\frac{2\pi n}{a}, \frac{2\pi m}{a})$, where m,n are integers, as we did in our considerations. In effect, the single-electron Hamiltonian can be recast in the matrix form for each spin, i.e.,

$$\hat{\mathcal{H}}_{\sigma} = \begin{pmatrix} \hat{c}_{\mathbf{k}\alpha,\sigma}^{\dagger} & \hat{c}_{\mathbf{k}\beta,\sigma}^{\dagger} \end{pmatrix} \begin{pmatrix} \epsilon_{\mathbf{k}}^{\alpha} & Z_{\mathbf{k}}^{\alpha\beta} \\ Z_{\mathbf{k}}^{\beta\alpha} & \epsilon_{\mathbf{k}}^{\beta} \end{pmatrix} \begin{pmatrix} \hat{c}_{\mathbf{k}\alpha,\sigma} \\ \hat{c}_{\mathbf{k}\beta,\sigma} \end{pmatrix} \equiv \mathbf{c}^{\dagger}\, \mathbb{H}\, \mathbf{c}. \tag{A3}$$

Diagonalization of matrix $\mathbb{H}$ provides the bare dispersion relation $\tilde{\epsilon}(\mathbf{k})$. For our 2D molecular crystal two, spin-degenerate, branches $\tilde{\epsilon}^{\mathrm{up}}(\mathbf{k})$ and $\tilde{\epsilon}^{\mathrm{down}}(\mathbf{k})$ appear. The matrix $\mathbb{H}$ is constructed in a straightforward manner for particular $\mathbf{k}$, i.e., by computing numerically $Z_k^{\mu\nu}$ with $\mathbf{r}_l^{\mu\nu}$ up to the 13th coordination zone. Subsequently, $\mathbb{H}$ is diagonalized and the two eigenvalues $\tilde{\epsilon}^{\mathrm{up}}(\mathbf{k})$, $\tilde{\epsilon}^{\mathrm{down}}(\mathbf{k})$ are obtained. For the *half filling* considered here, only $\tilde{\epsilon}^{\mathrm{down}}$ band is occupied by electrons. Therefore, W is defined in a standard manner, i.e.,

$$W = \tilde{\epsilon}_{\mathrm{max}}^{\mathrm{down}} - \tilde{\epsilon}_{\mathrm{min}}^{\mathrm{down}}. \tag{A4}$$

Both the maximal and the minimal values, $\tilde{\epsilon}_{\mathrm{max}}^{\mathrm{down}}$ and $\tilde{\epsilon}_{\mathrm{min}}^{\mathrm{down}}$, are obtained numerically for $\mathbf{k}$ by scanning the eigenvalues in the first Brillouin zone. Those values were used when plotting $U - W$ and U/W in Figs. 9 and 8 in the main text. Note that in the molecular state the lower band is nominally filled, whereas in the metallic state the bands overlap.

APPENDIX B: ASSESSMENT OF ZERO-POINT MOTION IN HARMONIC APPROXIMATION

We estimate the zero-point motion (ZPM) of our system by introducing a ion position uncertainty

$$\delta\mathbf{r} \equiv (\delta x, \delta y, \delta z), \tag{B1}$$

and then by splitting the problem into two parts: (i) ZPM in a molecule $[\delta\mathbf{r}_i \equiv (0,0,\delta z)]$; (ii) ZPM of a molecule in the crystal field $[\delta\mathbf{r}_{ii} \equiv (\delta x, \delta y, 0)]$. In both cases the kinetic energy of the H_2 molecule is

$$E_{\mathrm{kin}} \equiv 2\frac{\hbar^2 \delta\mathbf{p}^2}{2M}, \tag{B2}$$

where $\hbar \overset{a.u.}{\equiv} 1$, $M \overset{a.u.}{\equiv} 1836.15267247 \times \frac{1}{2}$, and $\delta\mathbf{p}$ is approximated via the Heisenberg uncertainty principle

$$\delta\mathbf{p}^2 \delta\mathbf{r}^2 \leqslant \frac{3\hbar^2}{4} \overset{est.}{\rightarrow} \delta\mathbf{p}^2 = \frac{3\hbar^2}{4\delta\mathbf{r}^2}. \tag{B3}$$

Hence $E_{\mathrm{kin}} = \frac{3\hbar^4}{4M\delta\mathbf{r}^2}$.

The potential energy is calculated separately for the cases (i) and (ii).

1. ZPM for H_2 molecule

We base our approach on our earlier work [20,39]. We define the potential

$$V_m(R,\delta\mathbf{r}_i) \equiv E(R+\delta z) - E_B, \tag{B4}$$

where $E(R)$ is the energy of the molecule of the molecular size R, and $E_B \equiv E(1.43042a_0)$, the minimum of energy for the static molecule (so that our potential used static equilibrium is a reference point).

The energy gain from the ionic movement is given by an expression

$$\begin{aligned}\Delta E(R,\delta\mathbf{r}_i) &= E_{\mathrm{kin}}(\delta\mathbf{r}_i) + V_m(R,\delta\mathbf{r}_i) \\ &= \frac{3\hbar^4}{4M\delta z^2} + E(R+\delta z) - E_B.\end{aligned} \tag{B5}$$

For the given molecular size R we minimize expression (B5) with respect to δz.

2. ZPM per molecule in the crystal

For the case of the molecule in the crystal field we assume that the electrons do not contribute to the ionic potential; hence

$$\begin{aligned}V_{\mathrm{crystal}}(a,R,\delta\mathbf{r}_i) \equiv &\sum_{\text{interaction cell}} \frac{e^2}{|\mathbf{R}_i(a) + (0,0,-R/2) - \delta\mathbf{r}|} \\ &+ \sum_{\text{interaction cell}} \frac{e^2}{|\mathbf{R}_i(a) + (0,0,R/2) - \delta\mathbf{r}|} \\ &- V_{\mathrm{static}}(a,R),\end{aligned} \tag{B6}$$

where a is the intermolecular distance, R is the molecule size, $e \overset{a.u.}{\equiv} \sqrt{2}$ is the charge of a hydrogen ion, *interaction cell* refers to the molecules we considered as our background (cf. Fig. 2 for the background considered in this paper) at the positions

TABLE III. Magnitude of the zero-point motion and all possible modes at the transitions and for the ambient pressure ($p = 0$). Energy values are in Rydbergs per molecule.

p (Ry/a_0^2)	Phase	a (a_0)	R_{eff} (a_0)	E_G (Ry)	E_{mode} (Ry)	Direction of the mode
0	Molecular I	4.3371	1.4031	−2.3858	2×0.01605	$(\pm\frac{1}{\sqrt{2}}, \pm\frac{1}{\sqrt{2}},0)$ or $(\pm\frac{1}{\sqrt{2}}, \mp\frac{1}{\sqrt{2}},0)$
					2×0.01608	$(\pm1,0,0)$ or $(0, \pm1,0)$
					0.01837	(0,0,1)
				$\mathbf{E_{ZPM}} =$	**0.08263 Ry**	$\mathbf{\lvert E_{ZPM}\rvert/\lvert E_G\rvert = 3.46\%}$
0.1102	Molecular I	2.7626	1.1511	−2.0674	2×0.03035	$(\pm\frac{1}{\sqrt{2}}, \pm\frac{1}{\sqrt{2}},0)$ and $(\pm\frac{1}{\sqrt{2}}, \mp\frac{1}{\sqrt{2}},0)$
					2×0.03044	$(\pm1,0,0)$ and $(0, \pm1,0)$
					0.00452	(0,0,1)
				$\mathbf{E_{ZPM}} =$	**0.1261 Ry**	$\mathbf{\lvert E_{ZPM}\rvert/\lvert E_G\rvert = 6.10\%}$
	Molecular II	2.6791	1.1881	−2.0173	2×0.03140	$(\pm\frac{1}{\sqrt{2}}, \pm\frac{1}{\sqrt{2}},0)$ and $(\pm\frac{1}{\sqrt{2}}, \mp\frac{1}{\sqrt{2}},0)$
					2×0.03150	$(\pm1,0,0)$ and $(0, \pm1,0)$
					0.00557	(0,0,1)
				$\mathbf{E_{ZPM}} =$	**0.13137 Ry**	$\mathbf{\lvert E_{ZPM}\rvert/\lvert E_G\rvert = 6.51\%}$
0.1954	Molecular II	2.4378	1.1296	−1.8362	2×0.03584	$(\pm\frac{1}{\sqrt{2}}, \pm\frac{1}{\sqrt{2}},0)$ and $(\pm\frac{1}{\sqrt{2}}, \mp\frac{1}{\sqrt{2}},0)$
					2×0.03596	$(\pm1,0,0)$ and $(0, \pm1,0)$
					0.00402	(0,0,1)
				$\mathbf{E_{ZPM}} =$	**0.14762 Ry**	$\mathbf{\lvert E_{ZPM}\rvert/\lvert E_G\rvert = 8.04\%}$
	Quasiatomic	2.2313	1.9281	−1.6478	2×0.03478	$(\pm\frac{1}{\sqrt{2}}, \pm\frac{1}{\sqrt{2}},0)$ and $(\pm\frac{1}{\sqrt{2}}, \mp\frac{1}{\sqrt{2}},0)$
					2×0.03493	$(\pm1,0,0)$ and $(0, \pm1,0)$
					0.00162	(0,0,1)
				$\mathbf{E_{ZPM}} =$	**0.14104 Ry**	$\mathbf{\lvert E_{ZPM}\rvert/\lvert E_G\rvert = 8.56\%}$

$\mathbf{R}_i(a)$, and $V_{\text{static}}(a,R)$ is the potential of static molecules,

$$V_{\text{static}}(a,R) \equiv \sum_{\text{interaction cell}} \frac{e^2}{|\mathbf{R}_i(a) + (0,0,-R/2)|} + \sum_{\text{interaction cell}} \frac{e^2}{|\mathbf{R}_i(a) + (0,0,R/2)|}. \tag{B7}$$

The energy gain from the ionic movement is given by an expression

$$\Delta E(R,\delta\mathbf{r}_{ii}) = E_{\text{kin}}(\delta\mathbf{r}_{ii}) + V_{\text{crystal}}(a,R,\delta\mathbf{r}_{ii}) = \frac{3\hbar^4}{4M(\delta x^2 + \delta y^2)} + V_{\text{crystal}}(a,R,(\delta x,\delta y,0)). \tag{B8}$$

For the given intermolecular distance a and molecular size R we minimize expression (B8) with respect to δx and δy.

3. Numerical results at the transitions

In Table III we present both absolute and relative magnitude of ZPM, as well as all the possible modes with their corresponding energies (in Rydberg per molecule).

[1] W. Kołos and L. Wolniewicz, Improved theoretical ground-state energy of the hydrogen molecule, J. Chem. Phys. **49**, 404 (1968).

[2] K. Pachucki and J. Komasa, Schrödinger equation solved for the hydrogen molecule with unprecedented accuracy, J. Chem. Phys. **144**, 164306 (2016).

[3] Ph. Dalladay-Simpson, R. T. Howie, and E. Gregoryanz, Evidence for a new phase of dense hydrogen above 325 gigapascals, Nature (London) **529**, 63 (2016).

[4] V. Dzyabura, M. Zaghoo, and I. F. Silvera, Evidence of a liquid–liquid phase transition in hot dense hydrogen, Proc. Natl. Acad. Sci. USA **110**, 8040 (2013).

[5] R. T. Howie, Ph. Dalladay-Simpson, and E. Gregoryanz, Raman spectroscopy of hot hydrogen above 200 GPa, Nat. Mater. **14**, 495 (2015).

[6] R. P. Dias and I. F. Silvera, Observation of the Wigner-Huntington transition to metallic hydrogen, Science **355**, 715 (2017).

[7] J. McMinis, R. C. Clay, D. Lee, and M. A. Morales, Molecular to Atomic Phase Transition in Hydrogen Under High Pressure, Phys. Rev. Lett. **114**, 105305 (2015).

[8] N. D. Drummond, B. Monserrat, J. H. Lloyd-Williams, P. López Ríos, Ch. J. Pickard, and R. J. Needs, Quantum Monte Carlo study of the phase diagram of solid molecular hydrogen at extreme pressures, Nat. Commun. **6**, 7794 (2015).

[9] E. Wigner and H. B. Huntington, On the possibility of a metallic modification of hydrogen, J. Chem. Phys. **3**, 764 (1935).

[10] M. I. Eremets and A. P. Drozdov, Comments on the claimed observation of the Wigner-Huntington transition to metallic hydrogen, arXiv:1702.05125.
[11] X.-D. Liu, Ph. Dalladay-Simpson, R. T. Howie, B. Li, and E. Gregoryanz, Comment on "Observation of the Wigner-Huntington transition to metallic hydrogen", arXiv:1704.07601.
[12] N. F. Mott, *Metal-Insulator Transitions* (Taylor & Francis, London, 1991).
[13] F. Gebhard, *The Mott Metal-Insulator Transition: Models and Methods* (Springer, Berlin, 1997).
[14] L. D. Landau and Y. B. Zeldovich, On the relation between the liquid and the gaseous states of metals, Acta Physicochim. URSS **18**, 194 (1943).
[15] L. D. Landau, *Collected Works* (Izdatyelstvo Nauka, Moscow, 1969), paper No. 48 (in Russian).
[16] S. Azadi and W. M. C. Foulkes, Fate of density functional theory in the study of high-pressure solid hydrogen, Phys. Rev. B **88**, 014115 (2013).
[17] A. P. Kądzielawa, A. Biborski, and J. Spałek, Discontinuous transition of molecular-hydrogen chain to the quasiatomic state: Combined exact diagonalization and *ab initio* approach, Phys. Rev. B **92**, 161101(R) (2015).
[18] A. Biborski, A. P. Kądzielawa, and J. Spałek, Combined shared and distributed memory *ab-initio* computations of molecular-hydrogen systems in the correlated state: Process pool solution and two-level parallelism, Comput. Phys. Commun. **197**, 7 (2015).
[19] A. P. Kądzielawa, J. Spałek, J. Kurzyk, and W. Wójcik, Extended Hubbard model with renormalized Wannier wave functions in the correlated state III, Eur. Phys. J. B **86**, 252 (2013).
[20] J. Spałek, R. Podsiadły, W. Wójcik, and A. Rycerz, Optimization of single-particle basis for exactly soluble models of correlated electrons, Phys. Rev. B **61**, 15676 (2000).
[21] J. Hubbard, Electron correlations in narrow energy bands, Proc. R. Soc. (London) **276**, 238 (1963).
[22] P. Fazekas, *Lecture Notes on Electron Correlation and Magnetism* (World Scientific, Singapore, 1999), Chaps. 8 and 9.
[23] P. Fulde, *Correlated Electrons in Quantum Matter* (World Scientific, Piscataway, NJ, 2012).
[24] A. L. Fetter and J. D. Walecka, *Quantum Theory of Many-Particle Systems* (Dover, Mineola, NY, 2003).
[25] A. Kądzielawa, A. Biborski, and J. Spałek (unpublished).
[26] J. Hubbard, Electron correlations in narrow energy bands. III. An improved solution, Proc. R. Soc. (London) **281**, 401 (1964).
[27] W. F. Brinkman and T. M. Rice, Application of Gutzwiller's variational method to the metal-insulator transition, Phys. Rev. B **2**, 4302 (1970).
[28] J. Spałek and W. Wójcik, Almost localized fermions and Mott-Hubbard transitions at non-zero temperature, in *Spectroscopy of Mott Insulators and Correlated Metals*, edited by A. Fujimori and Y. Tokura (Springer-Verlag, Berlin, 1995), pp. 41-65.
[29] D. Vollhardt, From Gutzwiller wave function to dynamical-field theory, in *DMFT ar 25: Infinite Dimensions*, edited by E. Pavarini *et al.* (Forschungszentrum, Jülich, 2014).
[30] J. Spałek, A. M. Oleś, and J. M. Honig, Metal-insulator transition and local moments in a narrow band: A simple thermodynamic theory, Phys. Rev. B **28**, 6802 (1983).
[31] N. F. Mott, On the transition to metallic conduction in semiconductors, Can. J. Phys. **34**, 1356 (1956).
[32] M. M. Maśka, Ground-state energy of the Hubbard model: Cluster-perturbative results, Phys. Rev. B **57**, 8755 (1998).
[33] S. T. Weir, A. C. Mitchell, and W. J. Nellis, Metallization of Fluid Molecular Hydrogen at 140 GPa (1.4 Mbar), Phys. Rev. Lett. **76**, 1860 (1996).
[34] I. Tamblyn and S. A. Bonev, Structure and Phase Boundaries of Compressed Liquid Hydrogen, Phys. Rev. Lett. **104**, 065702 (2010).
[35] M. A. Morales, C. Pierleoni, E. Schwegler, and D. M. Ceperley, Evidence for a first-order liquid-liquid transition in high-pressure hydrogen from *ab initio* simulations, Proc. Natl. Acad. Sci. USA **107**, 12799 (2010).
[36] I. F. Silvera, The insulator-metal transition in hydrogen, Proc. Natl. Acad. Sci. USA **107**, 12743 (2010).
[37] W. J. Nellis, Dynamic high pressure: Why it makes metallic fluid hydrogen, J. Phys. Chem. Solids **84**, 49 (2015).
[38] M. I. Eremets and I. A. Troyan, Conductive dense hydrogen, Nat. Mater. **10**, 927 (2011).
[39] A. Kądzielawa, A. Bielas, M. Acquarone, A. Biborski, M. M. Maśka, and J. Spałek, H_2 and $(H_2)_2$ molecules with an *ab initio* optimization of wave functions in correlated state: Electron–proton couplings and intermolecular microscopic parameters, New J. Phys. **16**, 123022 (2014).
[40] S. Azadi, N. D. Drummond, and W. M. C. Foulkes, Nature of the metallization transition in solid hydrogen, Phys. Rev. B **95**, 035142 (2017).
[41] J. M. McMahon and D. M. Ceperley, Ground-State Structures of Atomic Metallic Hydrogen, Phys. Rev. Lett. **106**, 165302 (2011).
[42] N. A. Kudryashov, A. A. Kutukov, and E. A. Mazur, Critical Temperature of Metallic Hydrogen at a Pressure of 500 GPa, Pis'ma v Zh. Eksp. Teor. Fiz. **104**, 488 (2016) [JETP Lett. **104**, 460 (2016)].
[43] M. Motta, D. M. Ceperley, G. Kin-Lic Chan, J. A. Gomez, E. Gull, Sh. Guo, C. Jimenez-Hoyos, T. N. Lan, J. Li, F. Ma, A. J. Millis, N. V. Prokof'ev, U. Ray, G. E. Scuseria, S. Sorella, E. M. Stoudenmire, Q. Sun, I. S. Tupitsyn, S. R. White, D. Zgid, and Sh. Zhang, Towards the solution of the many-electron problem in real materials: Equation of state of the hydrogen chain with state-of-the-art many-body methods, arXiv:1705.01608.
[44] J. Spałek, M. Zegrodnik, and J. Kaczmarczyk, Universal properties of high-temperature superconductors from real-space pairing: t-J-U model and its quantitative comparison with experiment, Phys. Rev. B **95**, 024506 (2017).
[45] M. Zegrodnik and J. Spałek, Effect of interlayer processes on the superconducting state within the t-j-u model: Full Gutzwiller wave-function solution and relation to experiment, Phys. Rev. B **95**, 024507 (2017).
[46] J. Kaczmarczyk, J. Spałek, T. Schickling, and J. Bünemann, Superconductivity in the two-dimensional Hubbard model: Gutzwiller wave function solution, Phys. Rev. B **88**, 115127 (2013).
[47] N. W. Ashcroft, Metallic Hydrogen: A High-Temperature Superconductor? Phys. Rev. Lett. **21**, 1748 (1968).
[48] M. Borinaga, I. Errea, M. Calandra, F. Mauri, and A. Bergara, Anharmonic effects in atomic hydrogen: Superconductivity and lattice dynamical stability, Phys. Rev. B **93**, 174308 (2016).